Frontiers in Heat and Mass Transfer

Tech Science Press

https://doi.org/10.32604/fhmt.2026.082573

ARTICLE

Graphical Analysis and 3D Thermodynamic Cycle Construction for Variable-Composition Ejector Refrigeration Cycle

Anxiang Shen[1], **Xinxin Ren**[2], **Tao Wang**[1] **and Jianqiu Zhou**[1,2,*]

[1]School of Mechanical and Power Engineering, Nanjing Tech University, No. 30 Puzhu Road(S), Nanjing, China
[2]School of Energy Science and Engineering, Nanjing Tech University, No. 30 Puzhu Road(S), Nanjing, China

*Corresponding Author: Jianqiu Zhou. Email: zhouj@njtech.edu.cn

Received: 19 March 2026; Accepted: 19 May 2026; Published: 31 August 2026

Highlights

- The relationship between working fluid properties and limiting LVSERC is derived.
- $COP_{limiting}$ is governed by $\Delta s_{b\text{-}b'}/\Delta s_{a\text{-}b'}$ and $\Delta s_{e\text{-}e'}/\Delta s_{d\text{-}e'}$.
- Graphical analysis is employed to reveal how fluid dryness/wetness affects COP.
- The effects of vapor quality and fluid composition are analyzed.

ABSTRACT: To address the growing number of variable-composition ejector refrigeration cycles, this study proposes analyzing the matching performance between working fluids and cycles through 3D (Temperature-Entropy-Mass fraction) Thermodynamic Diagrams. The ejector refrigeration cycle is decoupled into a driving module and a refrigeration module, and a theoretical upper-bound model ($COP_{limiting}$) that depends only on working-fluid properties is derived from the T-s diagram. Graph-theoretic analysis yields an explicit relation between $COP_{limiting}$ and fluid-specific parameters such as $\Delta s_{b\text{-}b'}/\Delta s_{a\text{-}b'}$ and $\Delta s_{e\text{-}e'}/\Delta s_{d\text{-}e'}$. Definition of k_1 ($\Delta T_{4-7}/\Delta s_{e\text{-}e'}$) and k_2 ($\Delta T_{3-4}/\Delta s_{b\text{-}b'}$) reveals that wet fluids favour the refrigeration module, whereas dry fluids favour the driving module. The influence of different mixtures has been also analyzed. The mixture of R227ea/R152a, R245fa/R134a, and Isobutane/pentane achieved their maximum $COP_{limiting}$ values at x = 0.5, 0.4, and 0.2, respectively. These optimal compositions all falling within the high-slope region of k_2. Additional parameters (x, t_g, t_c) are evaluated: At MF_t = 0.5, increasing x from 0.1 to 0.2 raises the limiting cycle COP from 0.08 to 0.18 and elevates t_e from −79.24°C to −35.15°C. Raising t_g from 85°C to 95°C lowers the limiting cycle COP from 0.1269 to 0.1235 while lifting t_e from −56.00°C to −49.18°C. Increasing t_c from 30°C to 40°C boosts the limiting cycle COP from 0.1216 to 0.1285 and raises t_e from −60.84°C to −44.26°C.

KEYWORDS: Ejector refrigeration cycle; limiting cycle; zeotropic mixture; graph theory

1 Introduction

According to estimates by the International Energy Agency, approximately 41% of global electricity consumption is attributed to the industrial sector [1]. Moreover, in heavy industries such as iron, steel, and chemical production, an estimated 20% to 50% of primary energy input is directly released into the environment as waste heat [2]. Consequently, over the past decade, governments worldwide have actively promoted sustainable energy development [3]. The ejector refrigeration cycle (depicted in Fig. 1a) has attracted research interest because it utilizes industrial waste heat as the driving source, thereby reducing electricity consumption during the refrigeration process. Nevertheless, the COP of ejector refrigeration cycles is generally low, which undoubtedly constrains their widespread adoption [4].

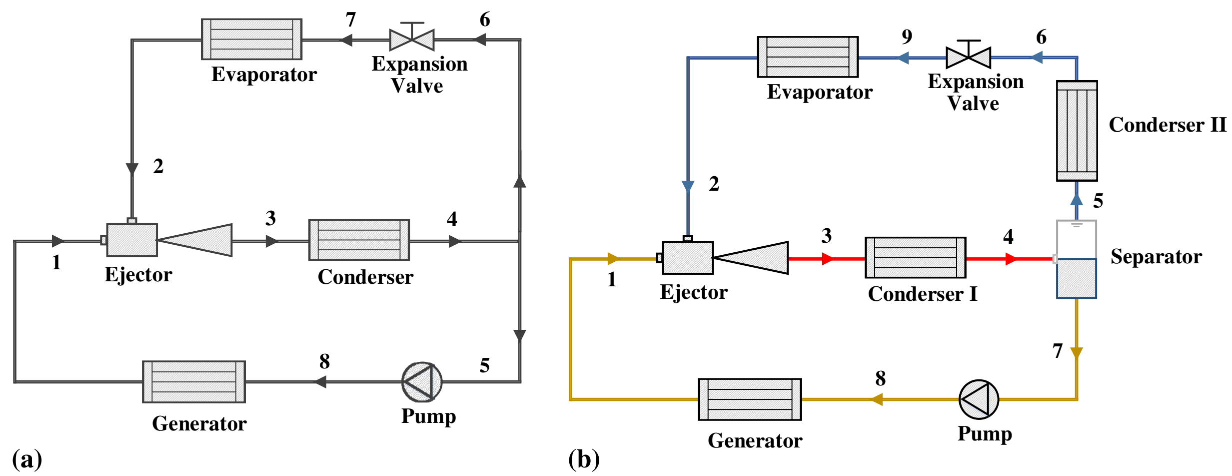

Figure 1: The ejector refrigeration cycle: (**a**) the traditional ejector refrigeration cycle (ERC); (**b**) the liquid-vapor separation condensation ejector refrigeration cycle (LVSERC).

Working fluid is crucial to the cycle performance, responsible for the transmission of power and the conveyance of energy within the system. Consequently, the thermophysical properties of the working fluid are of paramount importance to cycle performance. Sun [5] investigated the ejector refrigeration cycle utilizing various working fluids (water, R11, R12, R113, R123, R142b, R134a, and R152a) and comparatively evaluated their cycle performances, among which R152a demonstrated superior thermodynamic performance. Bellos and Tzivanidis [6] comparatively assessed the performance of R141b, R123, R245fa, R600a, and R134a in a solar-driven ejector refrigeration cycle, revealing the descending COP ranking: R141b > R123 > R245fa > R600a > R134a. Khaldi et al. [7] conducted a comparative analysis of R134a and R1234yf, demonstrating that R1234yf exhibits a significantly higher entrainment ratio. Kareem et al. [8] conducted a comparative simulation of twelve working fluids (R134a, R290, R1234yf, R600a, R1234ze, R410A, R152a, R227ea, R245h, R236fa, R407C, and R143a) in an ejector refrigeration cycle. The results indicated that R152a and R410A delivered the highest cycle performance, with R152a yielding a COP approximately 12.2% greater than that of R134a and 8.5% greater than that of R410A.

Zeotropic mixtures expand the working-fluid design space by virtue of their composition-dependent thermophysical properties. The use of zeotropic mixtures in ejector refrigeration systems can effectively reduce internal irreversibilities in heat exchange, thereby improving system efficiency [9]. In prior work [10], an ejector refrigeration cycle as shown in Fig. 1b employing R245fa and R134a as working fluids was proposed. The performance of this cycle is enhanced by varying the compositions of the primary and secondary flow. Yu and Yu [11] compared the cycle performances of R134a/R236fa and R1234yf/R245fa mixtures. They reported that the former raised the COP by 88.34% relative to the latter, underscoring the pronounced influence of mixture selection on COP. Liu et al. [9] evaluated eight mixtures (R123/R245fa, R245fa/R141b, R141b/RC318, R245fa/R134a, R245fa/R22, R141b/R134a, R245fa/R143a, and R141b/R22) in an ejector refrigeration cycle. The study identified the composition R245fa/R22 (0.3/0.7) as optimal, yielding a maximum COP of 0.293. Liang et al. [12] proposed a novel two-stage dual-temperature ejector refrigeration cycle employing R1234yf/R1234ze as the working fluid. The COP has enhanced by 5.64% when R1234yf mass fraction is 56.2%. Dai et al. [13] investigated a two-stage ejector refrigeration cycle utilizing R134a/R32 and R600a/R290 as working fluids; the maximum COP attained were 0.126 and 0.11, respectively.

Yan et al. [14] analyzed a modified ejector-expansion refrigeration cycle charged with R290/R600a; under identical operating conditions, the COP was elevated by 56%. Mosaffa and Garousi Farshi [15] proposed a parallel-connected combined ejector refrigeration and power system driven by geothermal energy. The two subsystems employed R601a/R600a and CO2/R32 as working fluids, respectively. Results demonstrated that the novel system achieved improvements of 3.9% and 4.8% in energy efficiency and exergy efficiency, respectively, compared to the basic system. Ye et al. [16] proposed a two-stage dual-temperature ejector auto-cascade refrigeration cycle (TEARC) driven by hot wastewater and low-pressure waste steam from chemical plants. The cycle employed R236fa/R236EA as the working fluid and was subjected to multi-objective optimization. Shi et al. [17] proposed a dual-ejector-enhanced two-stage auto-cascade refrigeration cycle for ultra-low temperature refrigeration. The cycle employed a ternary mixture of R600a/R41/R1150 as the working fluid. Compared with the baseline cycle, the new cycle achieved a COP improvement of 16.07%.

Furthermore, a number of researchers have systematized the criteria governing working-fluid selection. Kasperski and Gil [18] comparatively evaluated nine working fluids and concluded, from the perspective of the expansion process, that dry fluids are beneficial to cycle performance. This is attributed to the fact that a steeper slope of the saturation curve facilitates expansion into the superheated-vapor region; the steeper the saturation curve, the drier the fluid. Chen et al. [19] categorized working fluids into dry, wet, and isentropic fluids and performed numerical simulations for each; the results demonstrated that R600, classified as a dry fluid, delivered the optimum cycle performance. Mwesigye and Dworkin [20] emphasized that working-fluid selection must be tailored to the specific evaporation and condensation temperatures of the cycle. With the aim of mitigating irreversible losses induced by the pump, Xu et al. [21] proposed that working fluid screening should incorporate the dimensionless parameter $\alpha_V/(\rho c_p)$. Fu et al. [4] argued that cycle performance is governed by the parameters β and $\Delta s_{a\text{-}b}$ within the wet-fluid group R152a was identified as optimum, whereas R123 was superior among the dry fluids.

The selection of working fluids for conventional ejector refrigeration cycles has primarily relied on empirical matching of local thermodynamic processes, while the influence of the fluid on the remaining cycle processes is often neglected. To further enhance the matching between the working fluid and the cycle, numerous researchers have proposed ejector refrigeration cycles with variable-composition working fluids based on refrigerant screening, utilizing fluids with different compositions to match different processes within the cycle. Yu and Yu [11] proposed a flash separation working fluid ejector refrigeration cycle (FSRC). Simulation results showed that the FSRC using R290/R600a and R134a/R236fa achieved maximum COP improvements of 26.7% and 18.6%, respectively. Dai et al. [13] proposed a novel two-stage ejector refrigeration cycle (TSERC) utilizing a liquid-gas separator to separate low-boiling-point and high-boiling-point refrigerants, which outperforms conventional single-stage cycles. Zhao et al. [22] proposed an ejector refrigeration cycle with flash evaporation. When using R600a/R601a mixture as the working fluid, the maximum thermal efficiency reached 21.74%. Compared with pure R600a or R601a as working fluids, the performance was improved by 22.81% and 20.39%, respectively.

In summary, working fluid screening for ejector refrigeration cycles has traditionally focused on scenarios with fixed composition. However, the variable-composition characteristics of zeotropic mixtures significantly broaden the range of available working fluids, undoubtedly providing possibilities for matching fluid properties with individual cycle processes. Although numerous scholars have proposed various cycles with variable-composition working fluids, determining the appropriate composition to match thermodynamic processes in different components remains a challenge. Conventional thermodynamic methods, as shown in reference [4], typically employ two-dimensional temperature-entropy analysis, which is unsuitable for cycles with variable composition. By introducing additional dimensions such as composition and mass flow rate, the limitations of a single working fluid can be overcome, enabling multi-dimensional collaborative optimization in the T-s-composition domain, thereby providing new insights for constructing efficient cycles under complex heat source conditions.

Therefore, to fundamentally reveal the thermodynamic mechanism governing how the working fluid influences cycle performance and to provide theoretical criteria for subsequent working fluid selection and system optimization, this study constructs a limit cycle model subject solely to the thermodynamic property constraints of the working fluid. This model serves to characterize the thermodynamic limit performance of the system (limiting COP) achievable at a given heat source temperature through working fluid characteristic optimization alone. Subsequently, based on graph theory and multi-dimensional thermodynamic surface theory, thermodynamic analytical expressions for the driving module and refrigeration module are derived separately within the three-dimensional state space. By calculating the projected areas of the two modules on the diagram, the thermodynamic contribution of the working fluid in the ejector refrigeration cycle is quantitatively characterized, thereby clarifying the thermodynamic-level criteria for working fluid selection.

2 Methodology

2.1 Derivation of the Limiting Efficiency for a Three-Dimensional Ejector Refrigeration Cycle

As previously discussed [23], in the ERC the working fluids of the driving module and the refrigeration module are mixed within the ejector and subsequently separated at the condenser outlet, whereas in the LVSERC fluids of differing composition are blended in the ejector and then fractionated in the vapor-liquid separator. Consequently, the conventional T-s diagram shown in Fig. 2 represents merely the projected trajectories of the two modules. To rigorously capture the thermodynamic evolution of the fluid, the ejector cycle is first re-conceptualized as a coupling between a refrigeration module and a driving module, giving rise to a three-dimensional thermodynamic cycle. Leveraging this 3-D construct together with graphical analysis, closed-form expressions for the limiting cycle efficiencies of zeotropic-fluid ERC, zeotropic-fluid LVSERC, and pure-fluid cycles are derived in this section.

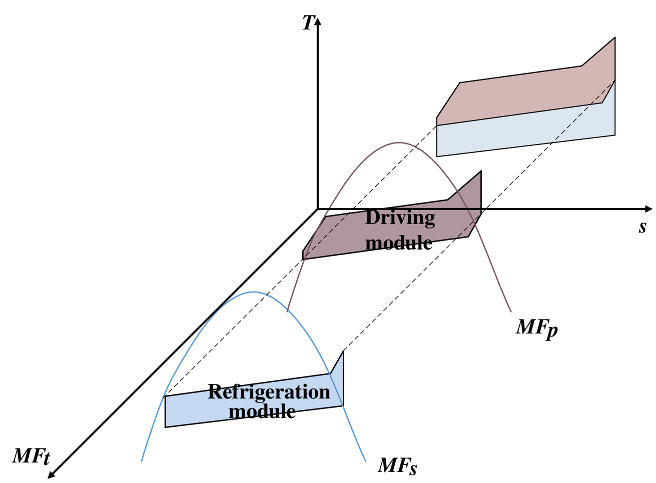

Figure 2: T-s-MF_t thermodynamic cycle schematic diagram of ERC.

Analogous to the limiting organic Rankine cycle [24,25], the limiting ejector refrigeration cycle derived in this study is intended to quantify the extent to which working-fluid properties constrain overall performance; consequently, it defines the theoretical upper bound attainable when the cycle is operated with a given fluid. It serves to quantify the thermodynamic role of the working fluid within the cycle. To expose this bound, the following idealizations are adopted:

(I) As previously established [23], the irreversible losses attributable to the pump, ejector, vapor–liquid separator, and throttling valve are negligible compared with other factors; consequently, all components are assumed to operate isentropically (efficiency = 1), and pressure drops as well as heat losses within equipment and piping are disregarded.
(II) Having neglected internal irreversibilities in both the ejector and the vapor-liquid separator, the physically mixed flow (the flow between the ejector outlet and the separator inlet) is conceptually decomposed into two thermally-interacting but compositionally distinct flow.
(III) The heat exchanger surface area is assumed to be infinite, thereby eliminating the irreversible loss associated with finite temperature differences during heat transfer.
(IV) The temperature profiles of the heat source and heat sink are assumed to track those of the working fluid exactly, eliminating any thermal mismatch irreversibility.
(V) Irreversibilities arising from the superheating of wet fluids and from the subsequent desuperheating of vapor inside the condenser are disregarded; the discarded exergy is illustrated by the shaded areas in Fig. 3a, and the thermodynamic path of the limiting cycle after this omission is shown in Fig. 3b.

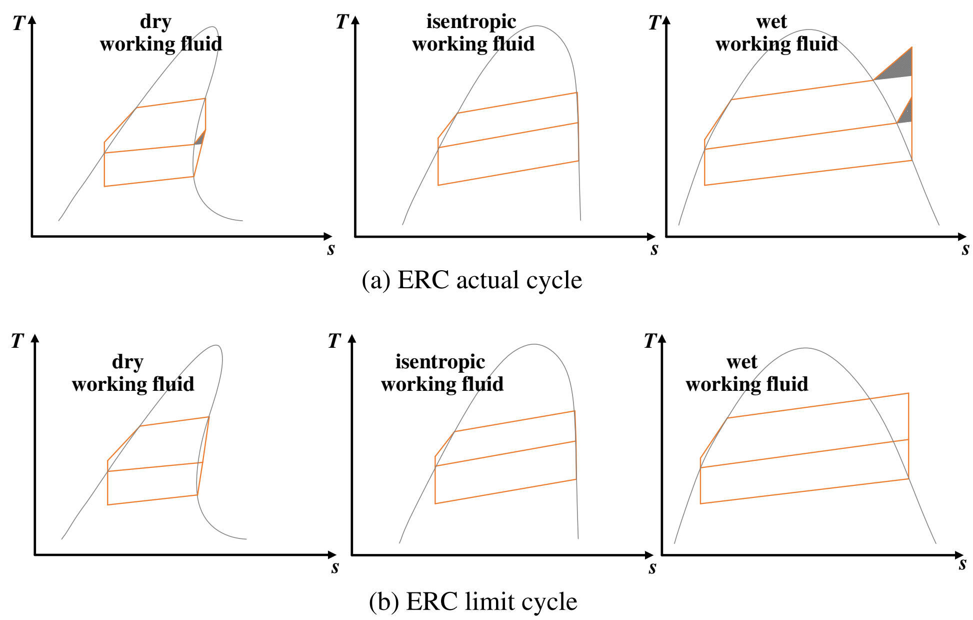

Figure 3: (**a**) The *T-s* diagram of ERC cycle for dry working fluid, isentropic working fluid and wet working fluid; (**b**) the *T-s* diagram of ERC limit cycle for dry working fluid, isentropic working fluid and wet working fluid.

2.1.1 COP of the Limiting Zeotropic LVSERC

For the limiting zeotropic LVSERC, the 3D *T-s* diagram is depicted in Fig. 4. To facilitate understanding, Fig. 5. presents the decoupled *T-s* diagram.

The driving module accelerates the primary flow (MF_g) through the nozzle, entraining the secondary flow (MF_e) from the refrigeration module; the two flows merge into a mixture of overall composition MF_t. After the first condensation, this mixture enters the vapor-liquid separator, where it is split into two flows of distinct compositions that are respectively recycled to the driving and refrigeration modules. Additionally, auxiliary points 4g and 4e are defined at the same pressure as Point 4, with entropies matching those of Points 3 and 7, respectively.

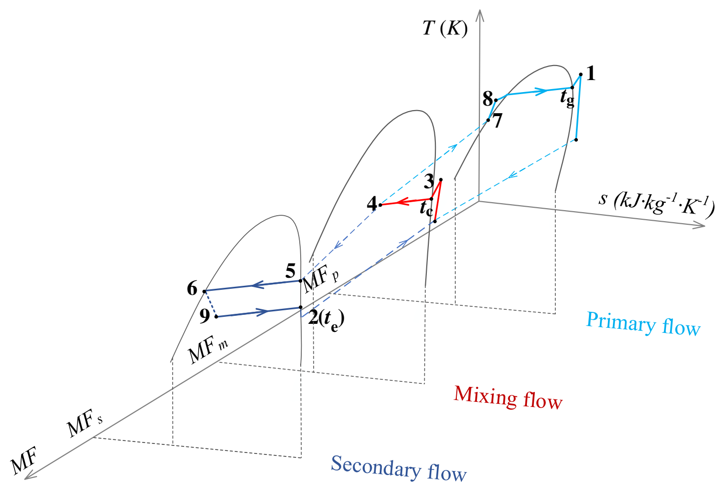

Figure 4: The 3D schematic for the LVSERC.

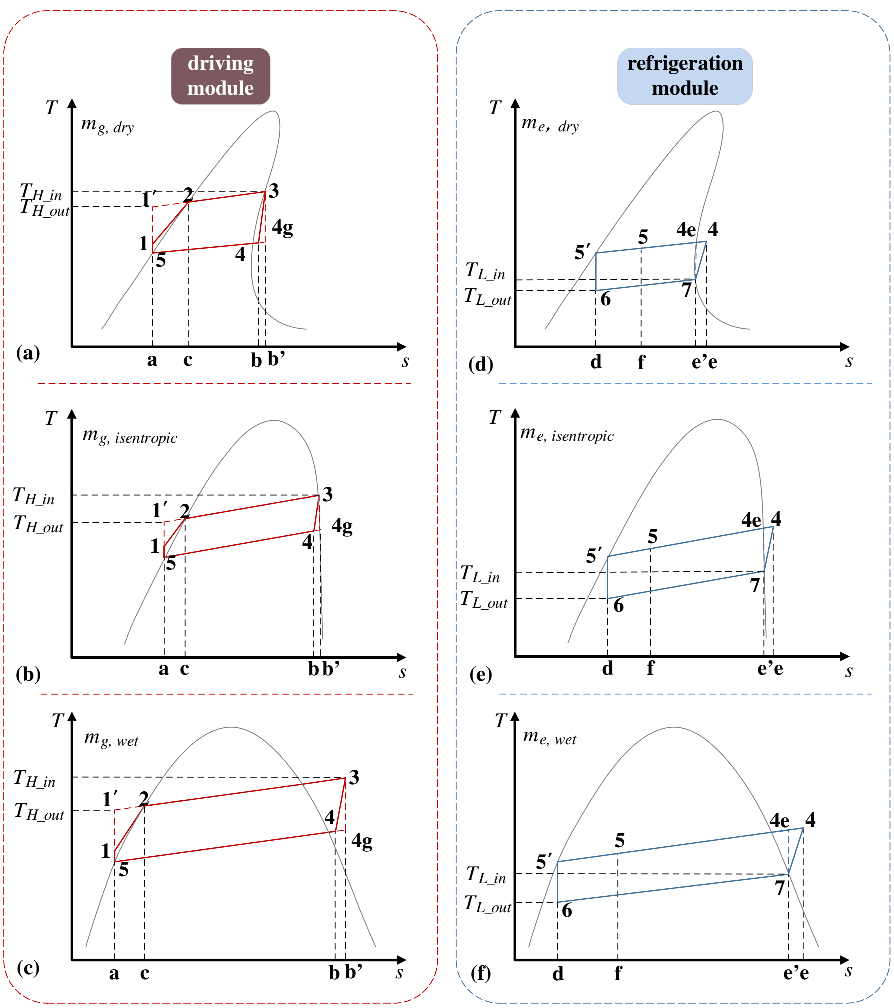

Figure 5: The T-s diagrams of the zeotropic mixtures LVSERC limit cycle after thermodynamic decoupling: (**a**) Driving module with dry fluid; (**b**) Driving module with isentropic fluid; (**c**) Driving module with wet fluid; (**d**) Refrigeration module with dry fluid; (**e**) Refrigeration module with isentropic fluid; (**f**) Refrigeration module with wet fluid.

Consequently, the driving and refrigeration modules are coupled through the principles of energy and mass conservation:

$$\mu = m_e/m_g \tag{1}$$

$$m_g q_g + m_e q_e = m_g q_{gc1} + m_e q_{ec1} + m_e q_{ec2} \tag{2}$$

$$m_e + m_g = m_t \tag{3}$$

where the left-hand side of Eq. (2) represents the heat absorbed by the evaporator and generator, and the right-hand side represents the heat rejected by the condenser.

On the basis of Eqs. (1)–(3), the entrainment ratio (μ) and the limiting coefficient of performance (COP_{limit_LVSERC}) for the zeotropic LVSERC are obtained as:

$$\mu = \frac{q_g - q_{gc1}}{q_{ec1} + q_{ec2} - q_e} \tag{4}$$

$$\begin{aligned} COP &= \frac{q_e}{q_g} \cdot \frac{\left(q_g - q_{gc1}\right)}{\left(q_{ec1} + q_{ec2} - q_e\right)} \\ &= \frac{q_e}{\left(q_{ec1} + q_{ec2} - q_e\right)} \cdot \frac{\left(q_g - q_{gc1}\right)}{q_g} \\ &= \frac{q_e}{\left(q_{ec1} + q_{ec2} - q_e\right)} \cdot \left(1 - \frac{q_{gc1}}{q_g}\right) \end{aligned} \tag{5}$$

Thermodynamic Analysis of the Driving Module

As shown in Fig. 5a–c, whether a dry, wet, or isentropic fluid, the specific heat absorbed per unit mass in the driving module is adopted-equals the area of pentagon (a-b'-4g-3-2-1-5-a), obtained by subtracting the area of triangle (1′-2-1-1′) from that of quadrilateral (a-b'-4g-3-2-1′-1-5-a). Owing to the negligible magnitude of pump work relative to the heat absorbed, the former is disregarded in the present analysis. Thus, the specific heat input to the driving module is expressed by Eq. (6):

$$q_g = A_{a-b'-4g-3-2-1'-1-5-a} - A_{1'-2-5-1'} \tag{6}$$

Although the straight line between point 2 and point 5 does not coincide exactly with the saturated-liquid curve, the deviation is negligible; consequently, it is approximated herein and assigned a slope β. Similarly, the line (1′-2-3) is characterized by a slope α. Thus, the area $A_{a\text{-}b'\text{-}4g\text{-}3\text{-}2\text{-}1'\text{-}1\text{-}5\text{-}a}$ can be expressed solely in terms of temperature and entropy, whereas $A_{1'\text{-}2\text{-}5\text{-}1'}$ is expressed as a function of temperature, entropy, and the slope β, as given by Eqs. (7) and (8):

$$A_{a-b'-4g-3-2-1'-1-5-a} = \frac{\left(T_{H\_out} + T_{H\_in}\right)}{2} \cdot \Delta s_{a-b'} \tag{7}$$

$$A_{1'-2-5-1'} = \frac{1}{2\beta} \cdot \left(T_2 - T_5\right)\left(T_{H\_out} - T_5\right) \tag{8}$$

Based on the definitions of β and α [Eqs. (9) and (10)], an expression for β solely in terms of temperature and entropy is obtained as Eq. (11):

$$\beta = \left(T_2 - T_5\right) \cdot \frac{1}{\Delta s_{a-c}} \tag{9}$$

$$\alpha = \left(T_2 - T_{H\_out}\right) \cdot \frac{1}{\Delta s_{a-c}} = \left(T_3 - T_{1'}\right) \cdot \frac{1}{\Delta s_{a-b'}} \tag{10}$$

$$\beta = \frac{\left(T_2 - T_5\right)\left(T_{H\_in} - T_{H\_out}\right)}{\left(T_2 - T_{H\_out}\right)} \cdot \frac{1}{\Delta s_{a-b'}} \tag{11}$$

Consequently, the area $A_{1'\text{-}2\text{-}5\text{-}1'}$ can be expressed as a function of temperature and entropy, as shown in Eq. (12):

$$A_{1'-2-5-1'} = \frac{\left(T_2 - T_{H\_out}\right)\left(T_{H\_out} - T_5\right)}{2\left(T_{H\_in} - T_{H\_out}\right)} \cdot \Delta s_{a-b'} \tag{12}$$

The specific heat absorbed per unit mass in the driving module can therefore be expressed as:

$$q_g = \left[\frac{\left(T_{H\_out} + T_{H\_in}\right)}{2} - \frac{\left(T_2 - T_{H\_out}\right)\left(T_{H\_out} - T_5\right)}{2\left(T_{H\_in} - T_{H\_out}\right)}\right] \cdot \Delta s_{a-b'} \tag{13}$$

The specific heat rejected per unit mass in the condenser of driving module corresponds to the area of quadrilateral (a-b'-4g-5-a) minus that of quadrilateral (a-b-4-5); it is therefore given by Eq. (14):

$$q_{gc1} = \frac{\left(T_5 + T_{4g}\right)}{2} \cdot \Delta s_{a-b'} - \frac{\left(T_4 + T_{4g}\right)}{2} \cdot \Delta s_{b-b'} \tag{14}$$

Thermodynamic Analysis of the Refrigeration Module

$$q_e = \frac{\left(T_{L\_in} + T_{L\_out}\right)}{2} \cdot \Delta s_{d-e'} \tag{15}$$

$$q_{ec1} + q_{ec2} = \frac{\left(T_{5'} + T_{4e}\right)}{2} \cdot \Delta s_{d-e'} + \frac{\left(T_{4e} + T_4\right)}{2} \cdot \Delta s_{e-e'} \tag{16}$$

$$\begin{aligned} COP &= \frac{q_e}{\left(q_{ec1} + q_{ec2} - q_e\right)} \cdot \left(1 - \frac{q_{gc1}}{q_g}\right) \\ &= \frac{\frac{\left(T_{L\_in} + T_{L\_out}\right)}{2} \cdot \Delta s_{d-e'}}{\frac{\left(T_{5'} + T_{4e}\right)}{2} \cdot \Delta s_{d-e'} + \frac{\left(T_{4e} + T_4\right)}{2} \cdot \Delta s_{e-e'} - \frac{\left(T_{L\_in} + T_{L\_out}\right)}{2} \cdot \Delta s_{d-e'}} \\ &\cdot \left\{1 - \frac{\frac{\left(T_5 + T_{4g}\right)}{2} \cdot \Delta s_{a-b'} - \frac{\left(T_4 + T_{4g}\right)}{2} \cdot \Delta s_{b-b'}}{\left[\frac{\left(T_{H\_out} + T_{H\_in}\right)}{2} - \frac{\left(T_2 - T_{H\_out}\right)\left(T_{H\_out} - T_5\right)}{2\left(T_{H\_out} - T_{H\_in}\right)}\right] \cdot \Delta s_{a-b'}}\right\} \\ &= \frac{\left(T_{L\_in} + T_{L\_out}\right)}{\left(T_{5'} + T_{4e}\right) + \left(T_{4e} + T_4\right) \cdot \frac{\Delta s_{e-e'}}{\Delta s_{d-e'}} - \left(T_{L\_in} + T_{L\_out}\right)} \\ &\cdot \left[1 - \frac{\left(T_5 + T_{4g}\right) - \left(T_4 + T_{4g}\right) \cdot \frac{\Delta s_{b-b'}}{\Delta s_{a-b'}}}{\left(T_{H\_out} + T_{H\_in}\right) - \frac{\left(T_2 - T_{H\_out}\right)\left(T_{H\_out} - T_5\right)}{\left(T_{H\_out} - T_{H\_in}\right)}}\right] \end{aligned} \tag{17}$$

As depicted in Fig. 5d–f, whether a dry, wet, or isentropic fluid is adopted, the refrigeration capacity per unit mass of the working fluid equals the area of quadrilateral (d-f-e'-7-6-d). The total heat rejected in the two condensers is given by the sum of the areas of quadrilateral (d-f-e-7-4e-5-5′-6-d) and quadrilateral (e'-e-4-4e-7-e'), with the latter also representing the heat absorbed by the refrigeration fluid in the ejector. Consequently, the specific refrigeration capacity and the aggregate condenser heat rejection can be expressed as:

In summary, substituting Eqs. (5) and (13)–(16) yields the closed-form analytical expression for the limiting COP of the zeotropic LVSERC, given by Eq. (17).

Eq. (17) indicates that, once the operating conditions are fixed, the limiting COP of the zeotropic LVSERC is governed by T_{4g}, T_{4e}, T_2, $\Delta s_{b\text{-}b'}/\Delta s_{a\text{-}b'}$ and $\Delta s_{e\text{-}e'}/\Delta s_{d\text{-}e'}$. Among these, T_{4g}, T_{4e}, $\Delta s_{e\text{-}e'}/\Delta s_{d\text{-}e'}$ and $\Delta s_{b\text{-}b'}/\Delta s_{a\text{-}b'}$ depend on the fluid composition at state 4 and on the component split between primary and secondary streams in the vapor-liquid separator, whereas T_2 is determined by the primary-stream composition.

2.1.2 COP of the Limiting Zeotropic ERC

The conventional zeotropic ERC cycle differs from the LVSERC in that no composition separation occurs; it can therefore be regarded as a limiting case of the LVSERC where the quality at the condenser outlet is zero. For the limiting zeotropic ERC, the 3D T-s diagram is depicted in Fig. 6. To facilitate understanding, Fig. 7 presents the decoupled T-s diagram.

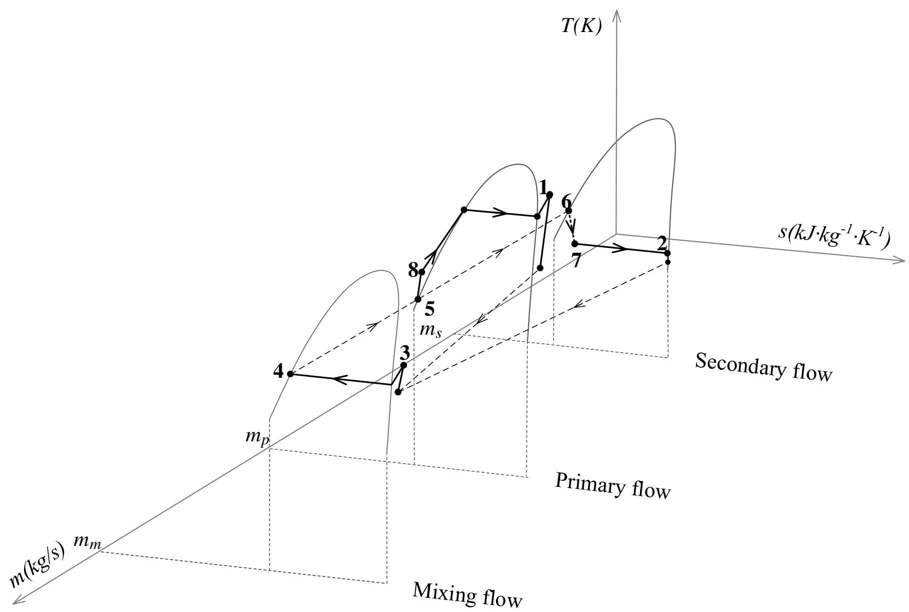

Figure 6: The 3D schematic for the ERC.

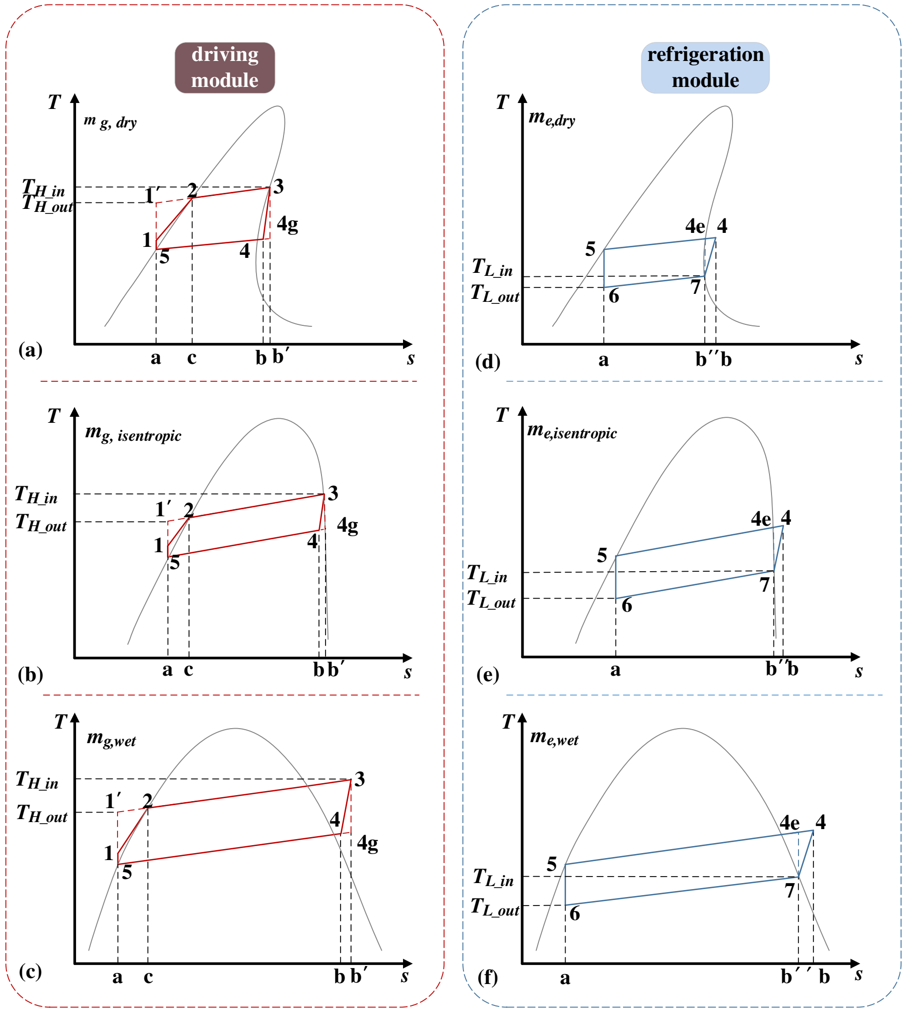

Figure 7: The T-s diagrams of the zeotropic mixtures ERC limit cycle after thermodynamic decoupling: (**a**) Driving module with dry fluid; (**b**) Driving module with isentropic fluid; (**c**) Driving module with wet fluid; (**d**) Refrigeration module with dry fluid; (**e**) Refrigeration module with isentropic fluid; (**f**) Refrigeration module with wet fluid.

In this configuration, the driving module accelerates the primary flow (m_g) through the nozzle, entraining the secondary flow (m_s) from the refrigeration module.

Consequently, its entrainment ratio and COP can be expressed as:

$$\mu = \frac{q_g - q_{gc}}{q_{ec} - q_e} \tag{18}$$

$$COP = \frac{q_e}{q_g} \cdot \frac{(q_g - q_{gc})}{(q_{ec} - q_e)} = \frac{q_e}{(q_{ec} - q_e)} \cdot \left(1 - \frac{q_{gc}}{q_g}\right) \tag{19}$$

The specific heat absorbed per unit mass in the driving module can thus be expressed as:

$$q_g = \left[\frac{(T_{H\_out} + T_{H\_in})}{2} - \frac{(T_2 - T_{H\_out})(T_{H\_out} - T_5)}{2(T_{H\_in} - T_{H\_out})}\right] \cdot \Delta s_{a-b'} \tag{20}$$

The specific heat rejected per unit mass in the driving module's condenser can be expressed by Eq. (21):

$$q_{gc} = \frac{(T_5 + T_{4g})}{2} \cdot \Delta s_{a-b'} - \frac{(T_4 + T_{4g})}{2} \cdot \Delta s_{b-b'} \tag{21}$$

The refrigeration module is equipped with a single condenser whose outlet temperature is identical to that of the driving-module condenser. Consequently, the specific refrigeration capacity and the specific heat rejection per unit mass of the refrigeration module can be expressed as:

$$q_e = \frac{(T_{L\_in} + T_{L\_out})}{2} \cdot \Delta s_{a-b''} \tag{22}$$

$$q_{ec} = \frac{(T_5 + T_{4e})}{2} \cdot \Delta s_{a-b''} + \frac{(T_{4e} + T_4)}{2} \cdot \Delta s_{b-b''} \tag{23}$$

$$\begin{aligned} COP &= \frac{q_e}{(q_{ec} - q_e)} \cdot \left(1 - \frac{q_{gc}}{q_g}\right) \\ &= \frac{(T_{L\_in} + T_{L\_out}) \cdot \Delta s_{a-b''}}{(T_5 + T_{4e}) \cdot \Delta s_{a-b''} + (T_{4e} + T_4) \cdot \Delta s_{b-b''} - (T_{L\_in} + T_{L\_out}) \cdot \Delta s_{a-b''}} \\ &\quad \cdot \left\{1 - \frac{(T_5 + T_{4g}) \cdot \Delta s_{a-b'} - (T_4 + T_{4g}) \cdot \Delta s_{b-b'}}{\left[(T_{H\_out} + T_{H\_in}) - \frac{(T_2 - T_{H\_out})(T_{H\_out} - T_5)}{(T_{H\_out} - T_{H\_in})}\right] \cdot \Delta s_{a-b'}}\right\} \\ &= \frac{(T_{L\_in} + T_{L\_out})}{(T_5 + T_{4e}) + (T_{4e} + T_4) \cdot \frac{\Delta s_{b-b''}}{\Delta s_{a-b''}} - (T_{L\_in} + T_{L\_out})} \\ &\quad \cdot \left[1 - \frac{(T_5 + T_{4g}) - (T_4 + T_{4g}) \cdot \frac{\Delta s_{b-b'}}{\Delta s_{a-b'}}}{(T_{H\_out} + T_{H\_in}) - \frac{(T_2 - T_{H\_out})(T_{H\_out} - T_5)}{(T_{H\_out} - T_{H\_in})}}\right] \end{aligned} \tag{24}$$

In summary, substituting Eqs. (19) and (20)–(23) yields the closed-form analytical expression for the limiting COP of the zeotropic ERC, given by Eq. (24).

2.1.3 COP of the Limiting Pure-Fluid ERC

Owing to the temperature glide of zeotropic mixtures, state $4e$ in the refrigeration module and state $4g$ in the driving module share only the same pressure, but not the same temperature. In contrast, for a pure fluid cycle, the temperatures at $4e$ and $4g$ are also identical.

Consequently, the specific heat absorbed per unit mass in the driving module of the limiting pure-fluid ERC can be expressed as:

$$q_g = T_H \cdot \Delta s_{a-b'} - \frac{1}{2\beta} \cdot (T_H - T_5)^2 \tag{25}$$

The specific heat rejected per unit mass in the driving-module condenser is given by Eq. (26):

$$q_{gc} = T_5 \cdot \Delta s_{a-b'} \tag{26}$$

The specific refrigeration capacity and the specific heat rejection per unit mass in the refrigeration module can be expressed as:

$$q_e = T_L \cdot \Delta s_{a-b'} \tag{27}$$

$$q_{ec} = T_5 \cdot \Delta s_{a-b'} \tag{28}$$

In summary, substituting Eqs. (19) and (25)–(28) yields the closed-form analytical expression for the limiting COP of the pure-fluid ERC, given by Eq. (29):

$$\begin{aligned} COP &= \frac{q_e}{(q_{ec} - q_e)} \cdot \left(1 - \frac{q_{gc}}{q_g}\right) \\ &= \frac{T_L}{T_5 - T_L} \cdot \left[1 - \frac{T_5}{T_H - \frac{1}{2\beta \cdot \Delta s_{a-b'}} \cdot (T_H - T_5)^2}\right] \end{aligned} \tag{29}$$

2.2 Working Fluid Selection

Working fluid is crucial to the cycle performance and it should match the cycle. This study used the working fluid previously studied [23] (a mixture of R245fa and R134a as the working fluid). The driving module absorbs heat from the source, expands in the ejector, and drives the refrigeration module. Dry fluids are more suitable for this main process. R245fa is a typical dry fluid whose effectiveness has been verified in ERC experiments, so it is selected as one component of the mixture. In contrast, the refrigeration module involves throttling and evaporation, processes for which wet fluids are preferable. R134a is a typical wet fluid that has been extensively studied in numerous simulations and experiments on ejector refrigeration cycles, and it is therefore chosen as the other mixture component. The thermodynamic properties of the fluids are the primary consideration. The property of the mixture components is listed in Table 1.

Table 1: The property of R245fa and R134a.

Fluid	P_{cr} (MPa)	t_{cr} (°C)	Boiling Point (°C)	ODP	GWP
R245fa	3.65	153.86	15.05	0	950 [26]
R134a	4.06	101.06	−26.07	0	1300 [26]

2.3 Model Validation

To validate the accuracy of the predictions by the model, the experimental results with R141b reported by Li et al. [27] are used. 11 different ejectors with different isentropic efficiencies of the diffuser and mixing section are compared in Table 2. Besides, the error with respect to the experimental results are also in Table 2.

Meanwhile, this study analyzes the applicability of the main working fluids (R134a and R245fa) in ejector refrigeration cycles. The comparison between the simulation results and the experimental data of R134a [27] is completed. As shown in Table 3, the results show that the maximum entrainment ratio error is 5.58%. The simulation results are compared with experimental data of R245fa [28], as shown in Table 4. The results show that the cycle COP error is 3% and the entrainment ratio error is 6.52%.

Table 2: Summary of calculated results and errors compared with experimental data of Li et al. [27].

η_m	η_d	T_g °C	T_e °C	P_c kPa	Entrainment Ratio Exp.	Entrainment Ratio cal.	Er (%)	Ar Exp.	Ar cal.	Er (%)
0.86	0.81	95	8	142.3	0.1859	0.1936	−4.14	6.44	6.3169	1.91
0.86	0.83	90	8	122.2	0.2718	0.2741	−0.85	6.99	6.6478	4.90
0.85	0.81	95	8	117.3	0.2814	0.3052	−8.46	8.28	8.0601	2.66
0.84	0.82	95	8	106.9	0.3457	0.3765	−8.91	9.41	8.9425	4.97
0.88	0.8	95	8	126.8	0.2552	0.273	−6.97	7.73	7.5036	2.93
0.81	0.84	95	8	127.6	0.2273	0.2341	−2.99	7.26	6.9519	4.24
0.87	0.81	95	8	120.5	0.2902	0.307	−5.79	8.25	7.9056	4.17
0.85	0.82	95	8	109.2	0.3505	0.3701	−5.59	9.17	8.776	4.30
0.84	0.83	95	8	104.7	0.3937	0.4048	−2.82	9.83	9.1561	6.86
0.85	0.82	95	8	137.3	0.2042	0.2128	−4.21	6.77	6.5476	3.29
0.85	0.82	95	8	98.6	0.4377	0.4615	−5.44	10.64	9.947	6.51

Table 3: Summary of calculated results and errors compared with experimental data of R134a [27].

T_g (°C)	T_e (°C)	T_c (°C)	Entrainment Ratio Exp.	Entrainment Ratio Cal.	Er (%)
75	10	33.7	0.1933	0.1875	−3.00
75	12.5	34.1	0.2209	0.2266	2.58
75	15	34.8	0.257	0.2617	1.83
80	10	36.6	0.1411	0.1484	5.17
80	12.5	36.9	0.1757	0.1855	5.58
80	15	37.9	0.2055	0.207	0.73

Table 4: Summary of calculated results and errors compared with experimental data of R245fa [28].

η_n	η_m	η_d	T_g (°C)	T_e (°C)	T_c (°C)
0.9	0.9	0.9	95	8	35
COP Exp.	**COP Cal.**	**Er (%)**	**Entrainment Ratio Exp.**	**Entrainment Ratio Cal.**	**Er (%)**
0.33	0.346	4.85	0.46	0.4358	5.26

Additionally, regarding the accuracy of the limiting cycle model, this study conducts a comparative investigation into the accuracy of the limiting cycle model when using different mixtures, as shown in Fig. 8 (t_g = 90°C, x = 0.15).

As can be seen from Fig. 8 the largest errors occur in q_{gc} and q_{ec}, which are attributed to the neglect of entropy generation during the fluid mixing process.

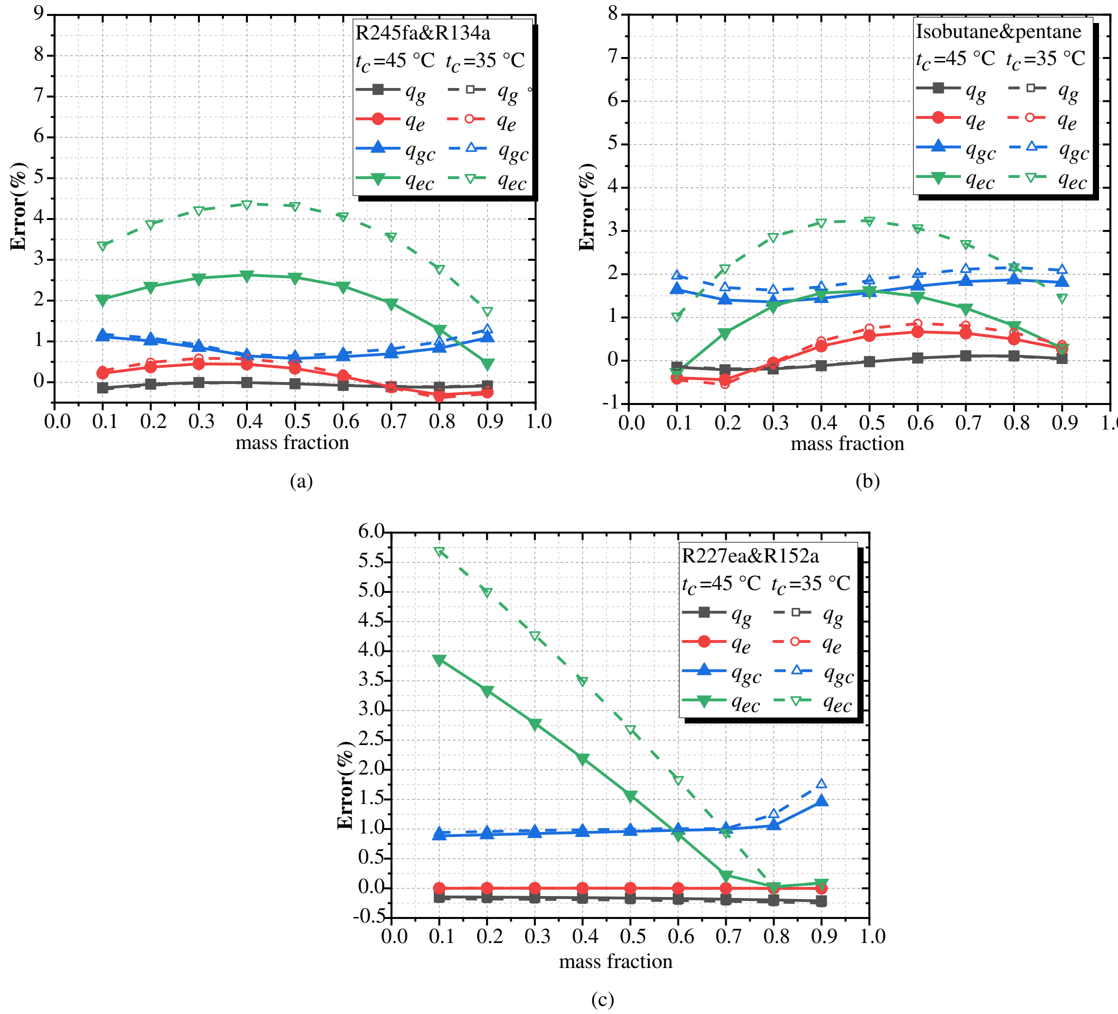

Figure 8: The accuracy of the limiting cycle model when using different mixtures. (**a**) R245fa & R134a; (**b**) Isobutane & pentane; (**c**) R227ea & R152a.

In addition, the manuscript also investigates the errors associated with the limit cycles for different working fluids. As shown in Fig. 9, when t_g = 90°C and t_c = 35°C, the errors are less than 10% in the vast majority of cases.

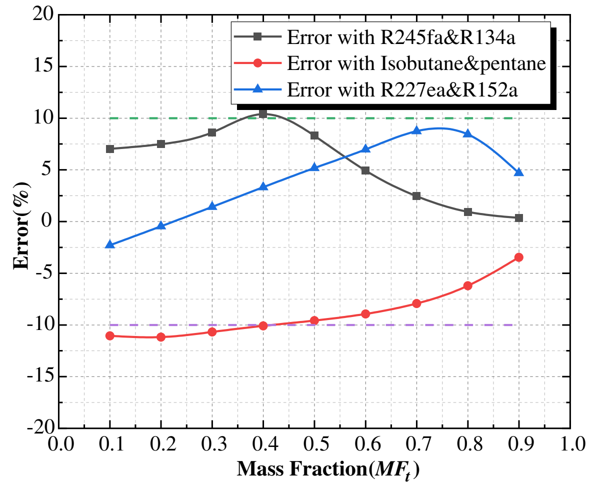

Figure 9: Errors with different working fluids.

3 Result and Discussion

3.1 Influence of Fluid Composition

Owing to its capability of regulating fluid composition, the LVSERC is selected as the exemplar for the first comparison between its limiting and actual cycles. The entrainment ratio of the ejector is associated with the thermodynamic states of the primary fluid, the secondary fluid, and the fluid at the ejector outlet. Notably, in the present study, it is also related to the separator. Accordingly, the state of the secondary fluid is determined from the fixed entrainment ratio, the primary fluid state, and the ejector outlet state. With respect to the ejector calculation, the same methodology as in previous studies is employed herein: an iterative approach. The calculation accounts for conservation of momentum, energy, and mass, as well as the Mach number, pressure, and area ratio, as that calculated in previous study [23]. For t_g = 90°C (the generator temperature) and t_c = 35°C (the condensation temperature), Fig. 10 shows that the limiting COP reaches a maximum of 0.1267 at a fluid composition (R245fa mass fraction) of approximately 0.4, while t_e attains its minimum value of −52.88°C at the vapor quality x = 0.5.

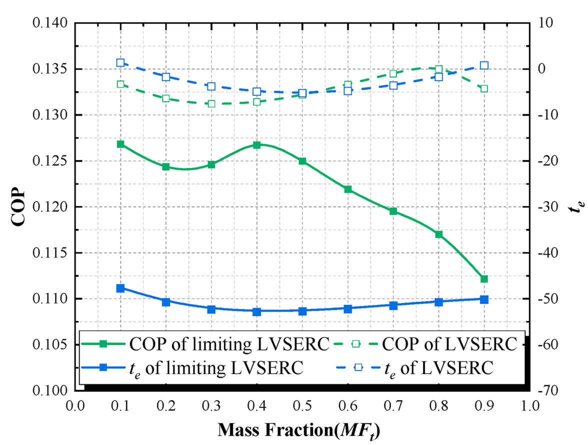

Figure 10: Effect of fluid composition on the limiting cycle COP and t_e.

As illustrated in the Fig. 11, the temperature drop of the heating fluid has been taken into account. As the component mass fraction increases from 0.1 to 0.9, the temperature glide in the vapor generator rises from 2.66°C to 10.26°C and then falls to 3.80°C, reaching its maximum at a mass fraction of 0.5. In addition, the latent heat of vaporization of the working fluid in the vapor generator initially increases and subsequently tends to level off. This behavior results from the combined effect of the temperature glide and the variation in composition. Therefore, a working fluid mass fraction of approximately 0.5 is optimal for the vapor generator, as it provides both a relatively large latent heat of vaporization and a large temperature glide.

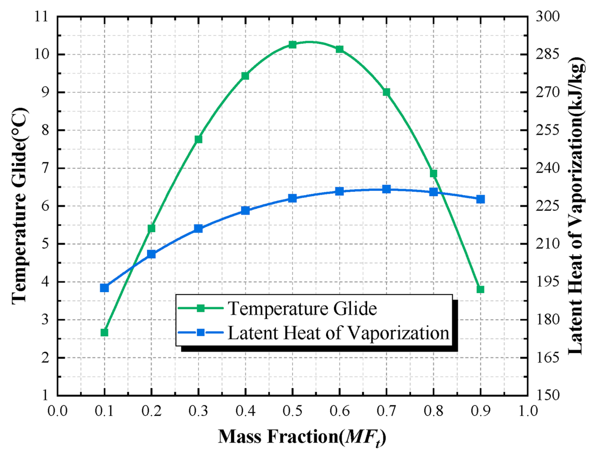

Figure 11: Effect of fluid composition on the temperature drop of the heating fluid.

As indicated by Eq. (17), the COP is influenced by $\Delta s_{b\text{-}b'}/\Delta s_{a\text{-}b'}$ and $\Delta s_{e\text{-}e'}/\Delta s_{d\text{-}e'}$. As shown in Fig. 12, both $\Delta s_{b\text{-}b'}/\Delta s_{a\text{-}b'}$ and $\Delta s_{e\text{-}e'}/\Delta s_{d\text{-}e'}$ increase as MF_t (the mass fraction of R245fa in the total fluid) rises from 0.1 to 0.9. The LVSERC limiting COP increases with $\Delta s_{b\text{-}b'}/\Delta s_{a\text{-}b'}$ but decreases with $\Delta s_{e\text{-}e'}/\Delta s_{d\text{-}e'}$. When both $\Delta s_{b\text{-}b'}/\Delta s_{a\text{-}b'}$ and $\Delta s_{e\text{-}e'}/\Delta s_{d\text{-}e'}$ increase simultaneously, the LVSERC limiting COP peaks at approximately 0.1267 for a fluid composition (R245fa mass fraction) of about 0.4.

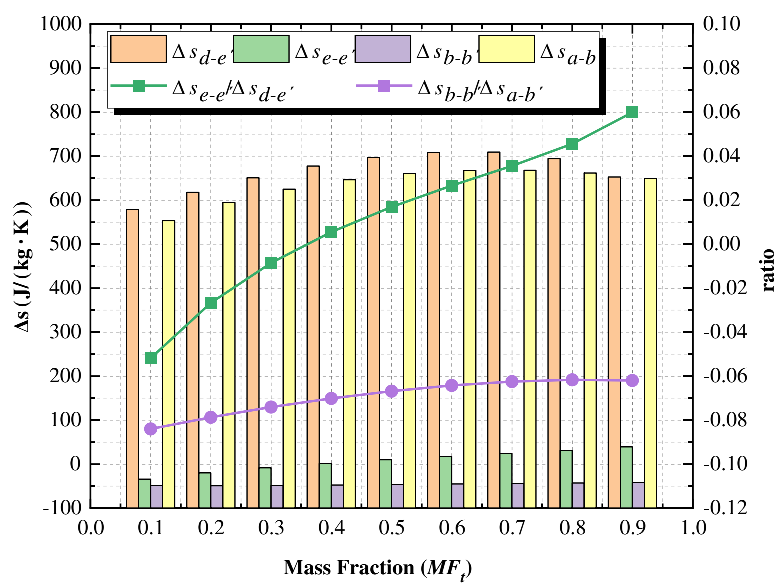

Figure 12: Effect of fluid composition on Δs.

The limiting COP of the LERC increases with increasing $\Delta s_{b\text{-}b'}/\Delta s_{a\text{-}b'}$, and decreases with increasing $\Delta s_{e\text{-}e'}/\Delta s_{d\text{-}e'}$. $\Delta s_{a\text{-}b'}$ represents the entropy difference across the generator (between inlet and outlet), and $\Delta s_{d\text{-}e'}$ represents the entropy difference across the evaporator (between inlet and outlet), as illustrated in Fig. 13 of the manuscript. $\Delta s_{b\text{-}b'}$ is the entropy difference across the driving module ejector (between inlet and outlet), and $\Delta s_{e\text{-}e'}$ is the entropy difference across the refrigeration module ejector (between inlet and outlet). Evidently, when the position of Point 4 changes, the variation in the entropy difference across the ejector is significantly greater than that across the heat exchanger. Therefore, the cycle performance is predominantly governed by the changes in the entropy difference across the ejectors ($\Delta s_{b\text{-}b'}$ and $\Delta s_{e\text{-}e'}$).

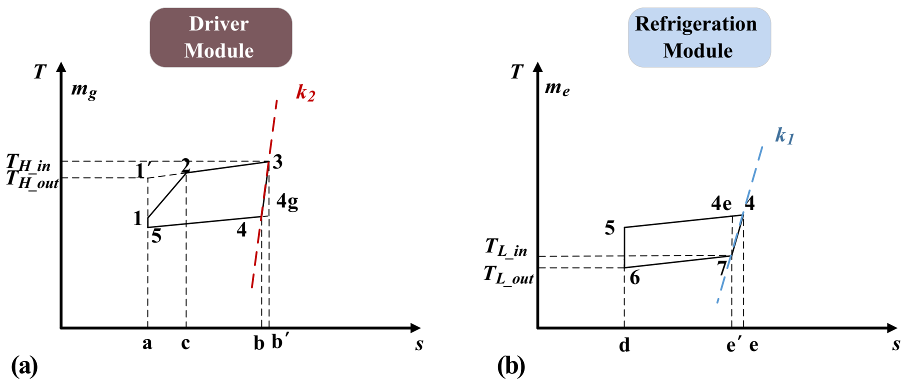

Figure 13: The *T-s* diagram of k_1 and k_2: (**a**) The *T-s* diagram of k_2;(**b**) The *T-s* diagram of k_1.

Therefore, to clarify the correlation between working fluid characteristics and cycle performance, slopes k_1 and k_2 are defined on the T-s diagram, as shown in Fig. 13. Specifically, k_1 is defined as the ratio of $\Delta T_{4\text{–}7}$ to $\Delta s_{e\text{-}e'}$, representing the slope of line 4–7 in the refrigeration module on the T-s diagram. k_2 is defined as the ratio of $\Delta T_{3\text{–}4}$ to $\Delta s_{b\text{-}b'}$, representing the slope of line 3–4 in the driving module on the T-s diagram. Since the working fluid exits the heat exchanger as saturated vapor, both Points 3 and 7 lie on the saturated vapor curve. As can be seen from the Eq. (17), an increase in $\Delta s_{e\text{-}e'}$ leads to a decrease in the limiting COP, and k_1 decreases accordingly. The saturated vapor curve also tilts in the same direction as k_1. Conversely, an increase in $\Delta s_{b\text{-}b'}$ leads to an increase in the limiting COP, while k_2 decreases. The saturated vapor curve also tilts in the same direction as k_2. Therefore, this is consistent with previous empirical conclusions: wet fluids are evidently more suitable for the refrigeration module, whereas dry fluids are better suited to the driving module.

Since the limiting cycle excludes every source of irreversibility except those intrinsic to the working fluid, the resultant refrigeration temperature is necessarily lower than that achievable in an actual cycle.

Furthermore, as shown in Fig. 14, this study also compared the effects of different working fluid combinations on cycle performance, as shown in Table 5. Three dry fluids (R227ea, R245fa, and Isobutane) and three wet fluids (R152a, R134a, and Pentane) were selected for investigation. This study aims to investigate the relationship between working fluid thermophysical properties and cycle performance. To ensure the accuracy of the thermophysical property parameters of the employed working fluid combinations and the universality of the observed trends, this study utilizes three classic working fluid combinations. Furthermore, the effect of the working fluid's dryness/wetness characteristics on the cycle performance is also considered in this study. Accordingly, the working fluid is a mixture of dry and wet fluids.

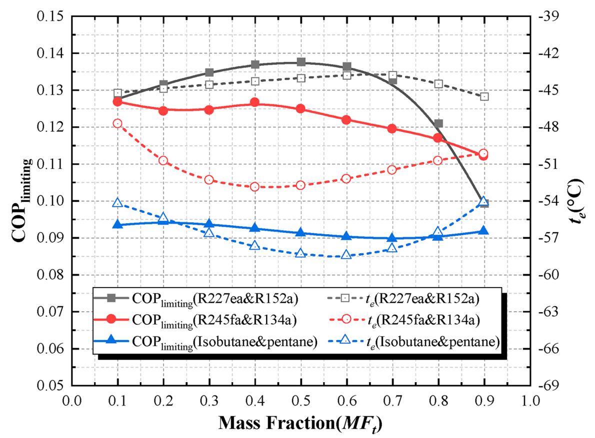

Figure 14: Effect of different mixtures on the limiting cycle COP and t_e.

Table 5: Thermophysical properties of fluids [4].

Working Fluids	Environmental and Safety Characteristics			Dryness/Wetness Characteristic
	ODP	GWP	Safety Classification	
R134a	0	1370	A1	Wet
R152a	0	133	A2	Wet
R290	0	20	A3	Wet
R227ea	0	3580	A1	Dry
R245fa	0	1050	B1	Dry
R600a	0	20	A3	Dry

When x is 0.5, the maximum $COP_{limiting}$ of 0.1377 is achieved by using R227ea and R152a. When x is 0.4, the maximum $COP_{limiting}$ of 0.1267 is obtained with R245fa and R134a. When x is 0.2, the maximum $COP_{limiting}$ of 0.0943 is reached using Isobutane and pentane. This trend is similar to that of k_2, as shown in Fig. 15, both falling within the high-slope region of k_2.

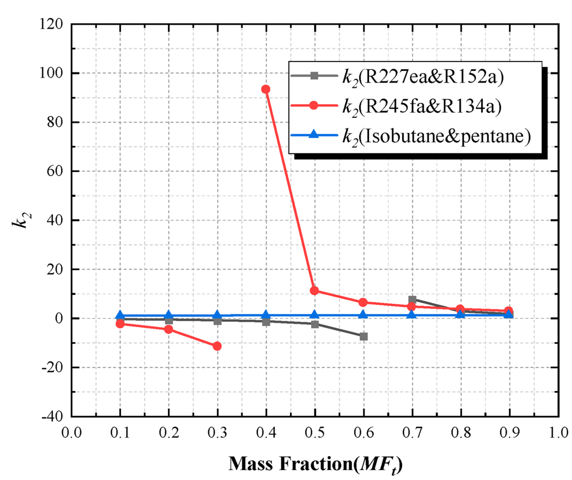

Figure 15: Effect of different mixtures on k_2.

3.2 Influence of Vapor Quality

Vapor quality, defined as the mass fraction at the outlet of condenser I, governs the cycle entrainment ratio. Its influence is illustrated in Figs. 16 and 17: at $MF_t = 0.5$, raising x from 0.1 to 0.2 increases the limiting cycle COP from 0.08 to 0.18 and raises t_e from −79.24°C to −35.15°C. This is because as the vapor quality increases, the cycle entrainment ratio also increases, which in turn raises the limiting COP. Furthermore, with increasing vapor quality, the working fluid temperature prior to the throttling process rises. Consequently, t_e increases.

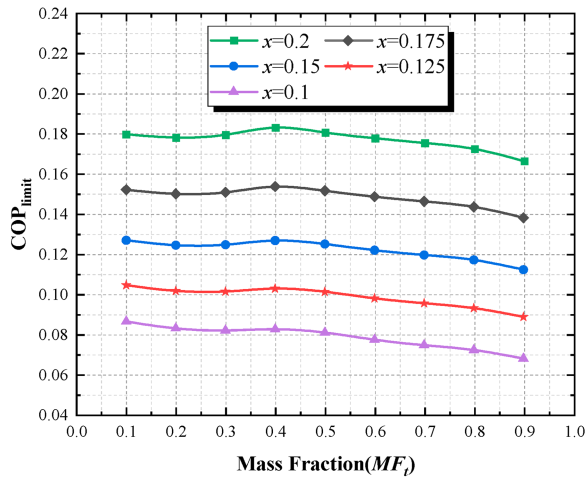

Figure 16: Influence of vapor quality on limiting cycle performance.

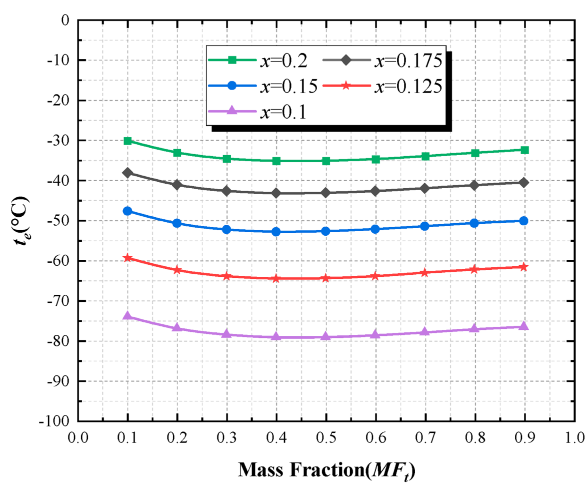

Figure 17: Influence of vapor quality on the limiting cycle refrigeration temperature.

3.3 Influence of Generation Temperature

As shown in Figs. 18 and 19, the generation temperature (t_g) influences both the limiting cycle efficiency and the refrigeration temperature (t_e). When $MF_t = 0.5$, increasing t_g from 85°C to 95°C reduces the limiting cycle COP from 0.1269 to 0.1235 and raises t_e from −56.00°C to −49.18°C.

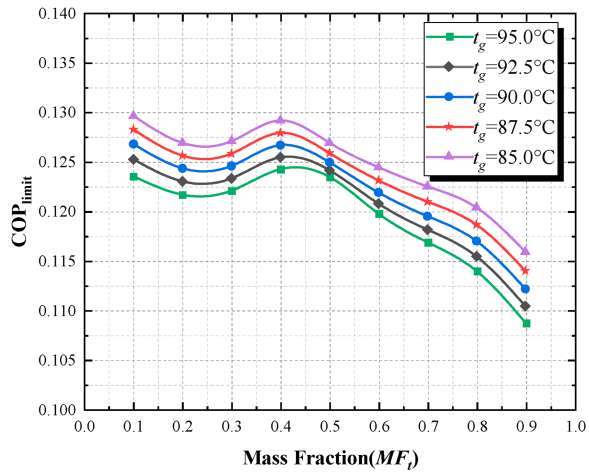

Figure 18: Influence of generation temperature on limiting cycle performance.

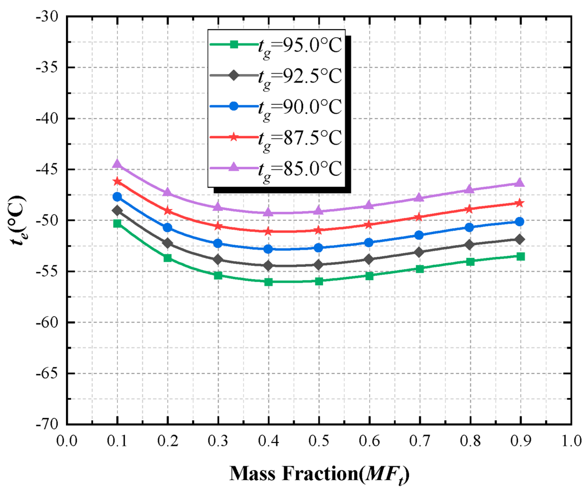

Figure 19: Influence of generation temperature on limiting cycle refrigeration temperature.

As previously mentioned, the ejector refrigeration cycle can be regarded as a coupling between the driving module and the refrigeration module. The efficiency of the driving module is related to the generator temperature (t_g) and the condensation temperature (t_c). As t_g increases while t_c remains constant, the efficiency of the driving module increases, and t_e decreases correspondingly. Similarly, the efficiency of the refrigeration module is related to t_c and t_e. As t_e decreases while t_c remains constant, the efficiency of the refrigeration module increases. Consequently, the COP increases with the increasing efficiencies of both the refrigeration module and the driving module.

In addition, as the generation temperature rises, the driving module exerts a stronger driving force on the refrigeration module, enabling a higher evaporation temperature to be achieved.

3.4 Influence of Condensation Temperature

As the intermediate temperature between the driving and refrigeration modules, the condensation temperature (t_c) exerts a pronounced influence on cycle performance. As illustrated in Figs. 20 and 21, when MF_t = 0.5, increasing t_c from 30°C to 40°C raises the limiting cycle COP from 0.1216 to 0.1285 and elevates

t_e from −60.84°C to −44.26°C. Higher condensation temperatures degrade the performance of the driving module, reducing the overall cooling capacity of the cycle and increasing the refrigeration temperature.

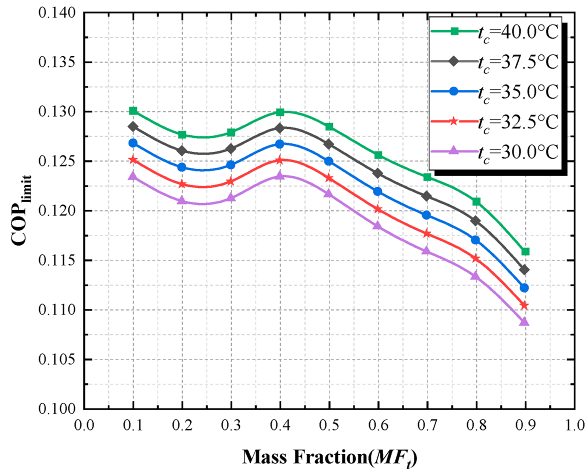

Figure 20: Influence of condensation temperature on limiting cycle performance.

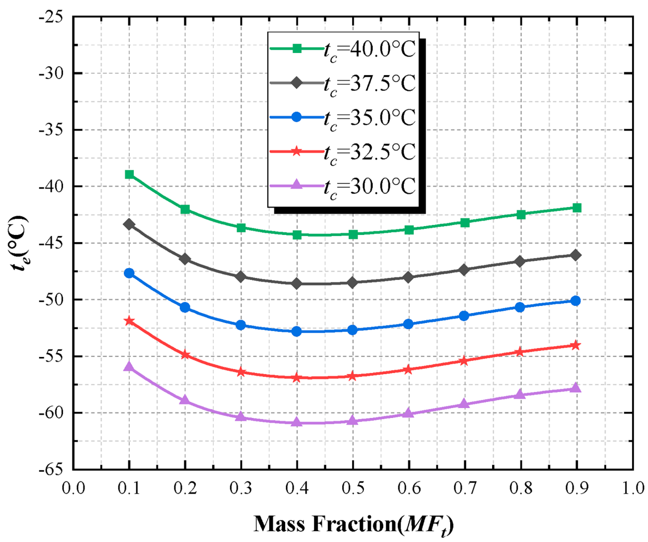

Figure 21: Influence of condensation temperature on limiting cycle refrigeration temperature.

Due to the function of the separator, the entrainment ratio remains constant. The cycle COP can be expressed as COP = $\mu \times (q_e/q_g)$. As t_c increases, the inlet temperature of the generator rises. However, since t_g remains unchanged, the pressure inside the generator stays constant. Heat transfer within the generator relies primarily on the vaporization process. The inlet of the vapor generator is liquid working fluid, and the temperature rise of the liquid working fluid has little effect on q_g. Moreover, as t_c increases, t_e also rises accordingly, and the pressure inside the evaporator changes. Consequently, q_e increases. In summary, COP increases as t_c increases.

4 Conclusion

This study focuses on the cycle with variable components and adopts a three-dimensional analysis method (temperature-entropy-mass fraction) for research. This study first decouples the factors influencing system performance to obtain a limiting cycle model governed solely by working fluid properties, thereby characterizing the theoretical performance bound attainable when only fluid characteristics are considered. Subsequently, three dimensional analytical expressions for zeotropic mixtures on the T-s-MF_t diagram are derived for both LVSERC and ERC systems through graph theoretic methods, quantifying the thermodynamic contribution of the fluid segment in ejector refrigeration cycles and establishing clear thermodynamic criteria for working fluid selection. Main conclusions are as follows.

(1) A limiting cycle framework for zeotropic-mixture ejector refrigeration is proposed. The cycle is first decoupled into a driving module and a refrigeration module; subsequently, graph-theoretic analysis is employed to derive the explicit relations between working-fluid properties and the limiting performance of the LVSERC, the zeotropic ERC, and the pure fluid ERC.

(2) Formula derivation shows that COP_{limiting} is governed by both working fluid intrinsic properties and operating temperatures. The fluid-specific contribution is captured by $\Delta s_{b\text{-}b'}/\Delta s_{a\text{-}b'}$ and $\Delta s_{e\text{-}e'}/\Delta s_{d\text{-}e'}$. Introduction of the physical parameters k_1 ($\Delta T_{4\text{–}7}/\Delta s_{e\text{-}e'}$) and k_2 ($\Delta T_{3\text{–}4}/\Delta s_{b\text{-}b'}$) and inspection of their slopes on the T-s diagram lead to the conclusion that wet fluids suit the refrigeration module, whereas dry fluids suit the driving module.

(3) The mixture of R227ea/R152a, R245fa/R134a, and Isobutane/pentane achieved their maximum COP_{limiting} values at x = 0.5, 0.4, and 0.2, respectively. These optimal compositions all falling within the high-slope region of k_2.

(4) Moreover, both the limiting cycle COP and the refrigeration temperature respond to t_g, and x rises, the COP falls and the refrigeration temperature drops, whereas an increase in t_c raises both the COP and the refrigeration temperature. Therefore, the maximum COP_{limiting} value with R245fa/R134a is at x = 0.2, MF_t = 0.4, t_g = 85°C and t_c = 40°C.

Acknowledgement: Not applicable.

Funding Statement: The authors received no specific funding for this study.

Author Contributions: The authors confirm contribution to the paper as follows: study conception and design: Anxiang Shen, Jianqiu Zhou; data collection: Xinxin Ren; analysis and interpretation of results: Tao wang; draft manuscript preparation: Anxiang Shen. All authors reviewed and approved the final version of the manuscript.

Availability of Data and Materials: The data are available from the corresponding author upon reasonable request.

Ethics Approval: Not applicable.

Conflicts of Interest: The authors declare no conflicts of interest.

Nomenclature

Symbols

COP	Coefficient of performance
LVSERC	Liquid-vapor separation condensation ejector refrigeration cycle
ERC	Ejector refrigeration cycle
m	Mass flow rate [kg·s^{-1}]
MF	The mass fraction of R245fa

s	Specific entropy [kJ·kg^{-1}·K^{-1}]
t	Temperature [°C]
x	Vapor quality
k	Slope
q	Unit heat exchange rate [kJ·kg^{-1}]

Greek Letters

μ	Entrainment ratio

Subscripts

c	Condenser or condensing
g	Generator or generating
e	Evaporator or evaporating
4g	Ejector outlet of driving module
4e	Ejector outlet of refrigeration module
gc	Condenser (driving module)
ec	Condenser (refrigeration module)
H	Heat source
L	Heat sink
t	Total
cr	Critical

References

1. Certeza LVRDT, Xiao X, Purnama AR, Low JSC, Lu WF. Optimal integration of a H_2O-LiBr absorption refrigeration system into an inter-plant heat exchange network. Energy Convers Manag. 2026;348(2):120781. doi:10.1016/j.enconman.2025.120781.
2. Jung HC, Krumdieck S, Vranjes T. Feasibility assessment of refinery waste heat-to-power conversion using an organic Rankine cycle. Energy Convers Manag. 2014;77(1):396–407. doi:10.1016/j.enconman.2013.09.057.
3. Yu J, Xia Y, Wang C, Yang J, Yan W, Jin S. Optimized improvement of double-stage solar AES saline wastewater treatment system based on performance simulation and exergy analysis. Desalination. 2024;578(6):117450. doi:10.1016/j.desal.2024.117450.
4. Fu J, Liu Z, Yang X, Jin S, Ye J. Limiting performance of the ejector refrigeration cycle with pure working fluids. Entropy. 2023;25(2):223. doi:10.3390/e25020223.
5. Sun DW. Comparative study of the performance of an ejector refrigeration cycle operating with various refrigerants. Energy Convers Manag. 1999;40(8):873–84. doi:10.1016/S0196-8904(98)00151-4.
6. Bellos E, Tzivanidis C. Optimum design of a solar ejector refrigeration system for various operating scenarios. Energy Convers Manag. 2017;154(1):11–24. doi:10.1016/j.enconman.2017.10.057.
7. Khaldi N, Sdiri S, Lazaar M. Thermodynamic analysis and optimization of an ejector refrigeration system for sustainable cooling applications. Int J Refrig. 2025;174(6):372–87. doi:10.1016/j.ijrefrig.2025.03.004.
8. Kareem FA, Alsayah AM, Alshukri MJ, Ali S, Faraj J, Khaled M. Advancing sustainable refrigeration: ejector expansion refrigeration cycles for energy efficiency and environmental protection. Results Eng. 2025;26(2):104926. doi:10.1016/j.rineng.2025.104926.
9. Liu B, Guo X, Xi X, Sun J, Zhang B, Yang Z. Thermodynamic analyses of ejector refrigeration cycle with zeotropic mixture. Energy. 2023;263(A):125989. doi:10.1016/j.energy.2022.125989.
10. Shen A, Guan K, Yang X, Jin S, Yang L. Theoretical analysis of a novel liquid-vapor separation condensation ejector refrigeration cycle with zeotropic mixtures. Energy Convers Manag. 2020;223(1):113322. doi:10.1016/j.enconman.2020.113322.
11. Yu M, Yu J. Thermodynamic analyses of a flash separation ejector refrigeration cycle with zeotropic mixture for cooling applications. Energy Convers Manag. 2021;229(2):113755. doi:10.1016/j.enconman.2020.113755.

12. Liang Y, Ye K, Zhu Y, Lu J. Thermodynamic analysis of two-stage and dual-temperature ejector refrigeration cycles driven by the waste heat of exhaust gas. Energy. 2023;278:127862. doi:10.1016/j.energy.2023.127862.
13. Dai Z, Chen X, Chen Q, Zhang X, Zhang H. Energy and exergy analysis of a novel two-stage ejector refrigeration cycle using binary zeotropic mixtures. Int J Refrig. 2024;168(6):178–89. doi:10.1016/j.ijrefrig.2024.08.016.
14. Yan G, Bai T, Yu J. Thermodynamic analysis on a modified ejector expansion refrigeration cycle with zeotropic mixture (R290/R600a) for freezers. Energy. 2016;95:144–54. doi:10.1016/j.energy.2015.11.067.
15. Mosaffa AH, Garousi Farshi L. Exergoeconomic analysis and optimization of a novel integrated two power/cooling cogeneration system using zeotropic mixtures. Energy. 2022;253:124132. doi:10.1016/j.energy.2022.124132.
16. Ye K, Liang Y, Zhu Y, Ling X, Wu J, Lu J. Performance improvement and multi-objective optimization of a two-stage and dual-temperature ejector auto-cascade refrigeration cycle driven by the waste heat. Energy. 2024;311:133429. doi:10.1016/j.energy.2024.133429.
17. Shi R, Bai T, Wan J. Performance analysis of a dual-ejector enhanced two-stage auto-cascade refrigeration cycle for ultra-low temperature refrigeration. Appl Therm Eng. 2024;240(205):122152. doi:10.1016/j.applthermaleng.2023.122152.
18. Kasperski J, Gil B. Performance estimation of ejector cycles using heavier hydrocarbon refrigerants. Appl Therm Eng. 2014;71(1):197–203. doi:10.1016/j.applthermaleng.2014.06.057.
19. Chen J, Havtun H, Palm B. Screening of working fluids for the ejector refrigeration system. Int J Refrig. 2014;47:1–14. doi:10.1016/j.ijrefrig.2014.07.016.
20. Mwesigye A, Dworkin SB. Performance analysis and optimization of an ejector refrigeration system using alternative working fluids under critical and subcritical operation modes. Energy Convers Manag. 2018;176:209–26. doi:10.1016/j.enconman.2018.09.021.
21. Xu W, Zhang J, Zhao L, Deng S, Zhang Y. Novel experimental research on the compression process in organic Rankine cycle (ORC). Energy Convers Manag. 2017;137:1–11. doi:10.1016/j.enconman.2017.01.025.
22. Zhao D, Xu W, Zhao R, Deng S, Zhao L. Thermodynamic analysis of the combined organic flash and ejector refrigeration cycle using zeotropic mixtures. Appl Therm Eng. 2023;219(9):119605. doi:10.1016/j.applthermaleng.2022.119605.
23. Su W, Zhao L, Deng S, Xu W, Yu Z. A limiting efficiency of subcritical Organic Rankine cycle under the constraint of working fluids. Energy. 2018;143:458–66. doi:10.1016/j.energy.2017.11.003.
24. Xu W, Deng S, Zhao L, Zhao D, Chen R. Identification of key affecting parameters of zeotropic working fluid on subcritical organic Rankine cycle according limiting thermodynamic cycle. Energy Convers Manag. 2019;197(1):111884. doi:10.1016/j.enconman.2019.111884.
25. Qi Y, Yang H, Zhang C. PρTx properties of binary R134a/R245fa system. J Chem Thermodyn. 2019;135(15):68–74. doi:10.1016/j.jct.2019.03.016.
26. Huang BJ, Chang JM, Wang CP, Petrenko VA. A 1-D analysis of ejector performance. Int J Refrig. 1999;22(5):354–64. doi:10.1016/s0140-7007(99)00004-3.
27. Li F, Li R, Li X, Tian Q. Experimental investigation on a R134a ejector refrigeration system under overall modes. Appl Therm Eng. 2018;137(1):784–91. doi:10.1016/j.applthermaleng.2018.03.102.
28. Chen J, Havtun H, Palm B. Investigation of ejectors in refrigeration system: optimum performance evaluation and ejector area ratios perspectives. Appl Therm Eng. 2014;64(1–2):182–91. doi:10.1016/j.applthermaleng.2013.12.034.